第133巻　第１号　2025年１月１日発行（毎月1回1日発行）　ISSN 1348-6535 CODEN:JCSJEW

JCS-Japan

January

vol.133

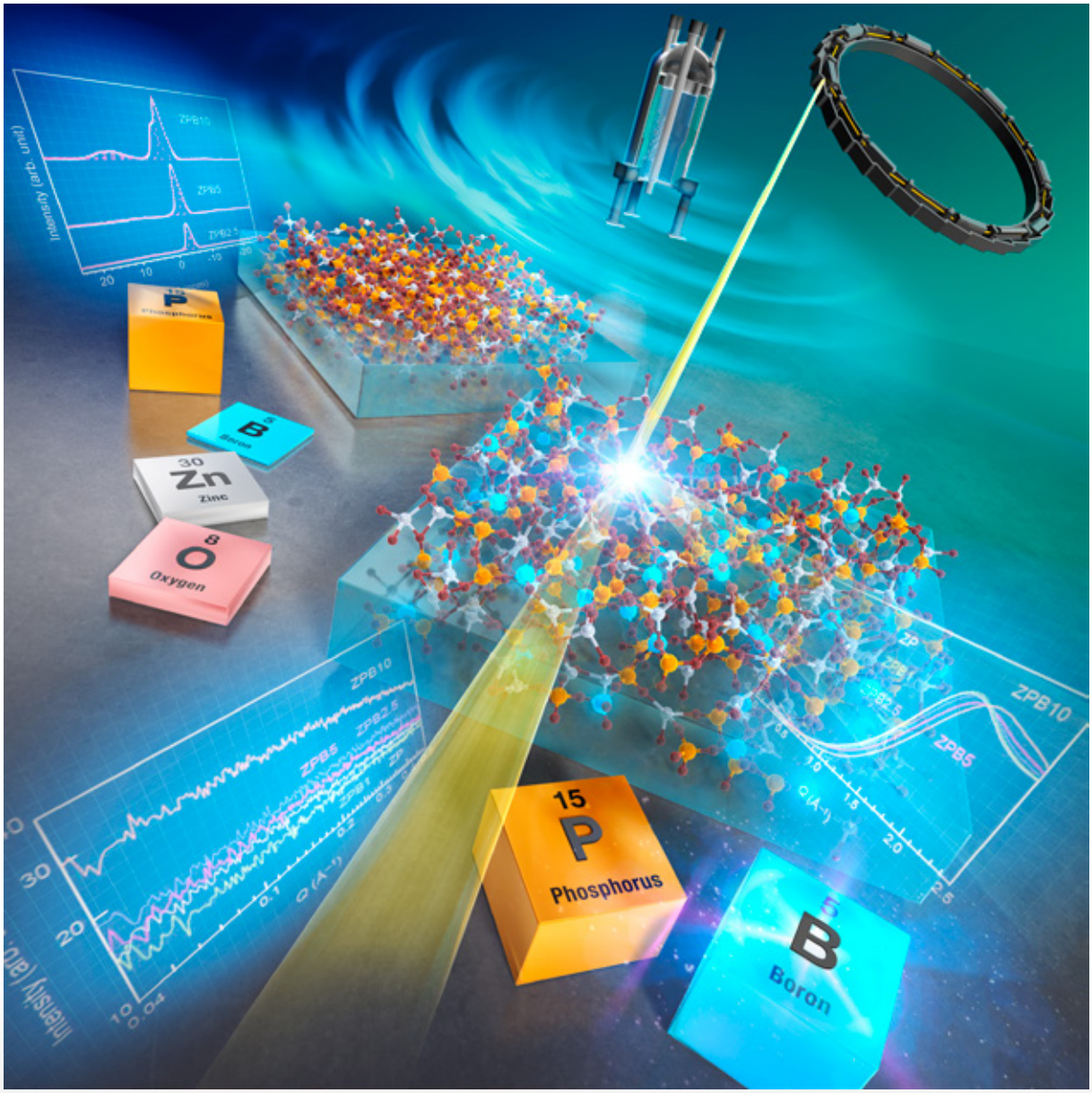

Journal of the Ceramic Society of Japan

2025

Journal of the Ceramic Society of Japan 133 [1] 1-8 2025
DOI https://doi.org/10.2109/jcersj2.24096

JCS-Japan

FULL PAPER

Effect of borate substitution on zinc phosphate glasses

Hirokazu Masai[1,†], Takahiro Ohkubo[2], Yohei Onodera[3], Yasuhiro Fujii[4,5], Seiya Shimono[6] and Akitoshi Koreeda[7]

[1]National Institute of Advanced Industrial Science and Technology, 1–8–31 Midorigaoka, Ikeda, Osaka 563–8577, Japan
[2]Graduate School & Faculty of Engineering, Chiba University, 1–33 Yayoi-cho, Chiba 263–8522, Japan
[3]Center for Basic Research on Materials, National Institute for Materials Science, 1–2–1 Sengen, Tsukuba, Ibaraki 305–0047, Japan
[4]Institute for Open and Transdisciplinary Research Initiatives, Osaka University, 2–1 Yamada-Oka, Suita, Osaka 565–0871, Japan
[5]Research Organization of Science and Technology, Ritsumeikan University, 1–1–1 Noji-higashi, Kusatsu, Shiga 525–8577, Japan
[6]Japan Synchrotron Radiation Research Institute (JASRI), 1–1–1 Kouto, Sayo-cho, Sayo-gun, Hyogo 679–5198, Japan
[7]Department of Physical Sciences, Ritsumeikan University, 1–1–1 Nojihigashi, Kusatsu, Shiga 525–8577, Japan

The combination of glass-forming oxides can induce phase separation at the atomistic level, particularly when a mixture involves both ionic and covalent bonds. In this study, we report physical properties of B_2O_3-substituted $ZnO–P_2O_5$ (ZP) glass and the substitution effect of B_2O_3 on the structure of ZP glasses via magic angle spinning nuclear magnetic resonance (MAS NMR), X-ray diffraction, small angle X-ray scattering, positron annihilation spectroscopy and inelastic light scattering measurements. The ^{11}B and ^{31}P MAS NMR results suggest that the coordination states of boron are affected by the number of bridging oxygen atoms in the substituted PO_4 chain structure of the ZP glass. At 5 mol % or less B_2O_3 substitution, an emerging of atomistic phase separation is not confirmed. On the contrary, at 10 mol % B_2O_3 substitution, three-coordinated boron formation is confirmed in ^{11}B MAS NMR in addition to a correlation between the $BO_{4/2}$ units. The substitution of a large amount of B_2O_3 confirmed the local coordination change of zinc cations in addition to the formation of a cluster-like structure in the low-Q region via small angle X-ray scattering.

Key-words : Glass, Phosphate, Borate, Structure, NMR, Diffraction, Inelastic light scattering

[Received August 31, 2024; Accepted October 13, 2024; Published online November 20, 2024]

1. Introduction

The metaloxane network connection in oxide glass is important not only for the vitrification of monolithic bulk glass without crystallization but also for the physical properties originating from the connectivity of constituting cation unit.[1)] Based on its glass-forming ability, SiO_2, GeO_2, B_2O_3, and P_2O_5 are classified as network former (NWF) units.[2)] However, because of the ionic P=O bond, P_2O_5 is different from other NWF units, and the structure of phosphate glass varies greatly depending on the chemical composition.[3–13)] The lower covalency of phosphate glass results in lower phonon vibrational energies compared with those of conventional silicate and borate glasses, which is advantageous for luminescence applications. In addition to lower phonon vibrational energy, the ionic phosphate units have a high affinity for active cations, allowing for a more uniform distribution and higher doping of active cations compared to conventional SiO_2 or B_2O_3 glasses. Therefore, phosphate glasses are sometimes used as a host material for activators.[14–18)]

It has been reported that the connectivity of the constituents of glassy materials is not homogeneous from an atomistic point of view, even in pristine SiO_2 glass.[19)] If there are different metaloxane units exhibiting different covalent/ionic bonds, they tend to phase separate, at least atomistic level. The phase separation is a kind of thermodynamically stabilization processes for liquids, and it generally accelerates crystallization of glass. The conventional spinodal phase separation is often observed in multicomponent glass where ionic and covalently bonded units coexists. The phase separation is a density fluctuation of components of a glass, often leading to a loss of optical transparency.

It was reported that $60ZnO–(40-x)P_2O_5–xB_2O_3$ glass exhibits macroscopic phase separation or crystallization at the intermediate chemical compositions.[18)] In the paper, Sn^{2+} was used as an activator, whose luminescent properties depend on the chemical composition of glass, i.e. fractions of P_2O_5 and B_2O_3. Since Sn^{2+} possesses the electrons in the outermost shell in both ground and excitation states, the luminescence is strongly affected by the surrounding region. In other words, the luminescence of Sn^{2+} is considered to be an indicator for the local structure of glass. However, detailed structures, such as the structural rela-

† Corresponding author: H. Masai; E-mail: hirokazu.masai@aist.go.jp

Table 1. Physical parameters of the ZPBx glass. The sound velocities were calculated using values of the Brillouin shift ν_B and refractive index of incident light (532 nm)

B_2O_3 fraction (mol %)	ID	T_g (°C) (±3 °C)	Molar volume ($cm^3\,mol^{-1}$)	Refractive index at 532 nm (±0.0003)	Longitudinal sound velocity ($m\,s^{-1}$) (±1 $m\,s^{-1}$)	C_{11} (GPa)
0	ZP	421	32.39	1.5792	4,563	66.59
1.0	ZPB1	420	31.95	1.5821	4,570	68.56
2.5	ZPB2.5	422	30.97	1.5906	4,686	73.59
5.0	ZPB5	426	30.04	1.6040	4,869	80.52
10.0	ZPB10	475	28.02	1.6213	5,112	91.78

tionships among the phosphate and borate units, have not been fully clarified. For example, it is not clear whether atomistic phase separation[20,21] (not a conventional macroscopic phase separation observable by naked eyes) occurs in $ZnO–P_2O_5–B_2O_3$ glasses containing small fraction of B_2O_3.

Recently, we reported the three-dimensional (3-D) structure of binary zinc phosphate (ZP) glasses consisting of ZnO (intermediate group) and phosphate units constructed by reverse Monte Carlo modeling based on ^{31}P nuclear magnetic resonance (NMR), neutron and X-ray diffraction, and Zn K-edge X-ray absorption fine structure (XAFS).[22] Based on various data obtained by different measurement techniques, we find that the main phosphate network was substituted by an intermediate ZnO subnetwork, depending on the chemical composition. Therefore, combinatorial characterization is important to investigate the structure of glasses.[22–26]

Here, we examined B_2O_3-substituted ZP glasses and the composition-dependent structures using a combination of inelastic light scattering, positron annihilation spectroscopy, solid-state magic angle spinning (MAS) NMR, X-ray diffraction, and small angle X-ray scattering. We focused on the atomistic phase separation behavior of B_2O_3-substituted ZP glasses and the correlation of data obtained using different measurement techniques.

2. Experimental

2.1 Preparation of B_2O_3-substituted ternary zinc phosphate glasses

Ternary $60ZnO–(40-x)P_2O_5–xB_2O_3$ (ZPBx) glasses ($x = 0$, 1, 2.5, 5, and 10) were prepared via a conventional melt-quenching method using a platinum crucible.[27] Batches comprising ZnO (99.99 %), $(NH_4)_2HPO_4$ (99 %), and B_2O_3 (99.9 %) were initially calcined at 800 °C for 3 h in an ambient atmosphere. The calcined solid was then melted at 1,100 °C for 30 min in the ambient atmosphere. The glass melt was quenched on a stainless-steel plate maintained at approximately 200 °C and then annealed at the glass transition temperature T_g for 1 h. The samples were mechanically polished to obtain mirror surfaces. The sample sizes were approximately 10 mm × 10 mm × 1 mm for the optical measurements.

2.2 Analysis methods

T_g was determined using a differential thermal analysis (DTA) system operating at a heating rate of 10 °C/min using a TG8120 (Rigaku, Japan). The densities were measured using the Archimedes method with water at the room temperature. We measured the refractive indices of the samples using a prism coupler with 473, 633, 1,319, and 1,553 nm light sources (Metricon, N.J., U.S.A.). The error in the measurement was 10^{-4}.

The Brillouin shifts ν_B of the glasses were measured using the high-resolution modification of a Sandercock FP system.[28] The excitation laser was a frequency-doubled diode-pumped solid-state (DPSS) Nd: yttrium-aluminum-garnet laser oscillating in a single longitudinal mode at 532 nm (Oxxius SLIM-532 300 mW). In addition to the excitation laser source, a second weak reference laser was employed as an independent reference signal to stabilize the FP. The reference laser was a small DPSS Nd: yttrium-vanadate (Nd:YVO_4) laser module (Photonic Products 300-0088-01, 4 mW) oscillating in a single transverse mode (TEM00), with two to three longitudinal modes separated by 120 GHz. The longitudinal sound velocities V_L listed in **Table 1** were calculated using the relation $V_L = \nu_B\lambda/2n_{532}$, where ν_B, λ, and n_{532} are the Brillouin shift, wavelength of the incident light (= 532 nm), and refractive index at 532 nm, respectively. The n_{532} values were calculated using the Cauchy relation with the refractive indices at different wavelengths.

Positron annihilation lifetime measurements were performed using a PSA TypeL-II (Toyo Seiko Co., Ltd.). The ^{22}Na source, which was encapsulated with Kapton® film, was used for measurement.[29] The accumulated counts for each sample was 10^7.

^{31}P and ^{11}B MAS NMR spectra were obtained to examine the local coordination states of each metal oxide. The ^{31}P MAS NMR spectra of the glasses were acquired on a DELTA 600 spectrometer (JEOL, Japan) at a frequency of 242.95 MHz with 15 kHz spinning rate and 500 s relaxation delay for 16 scans. The chemical shifts were estimated with respect to an 85 % H_3PO_4 aqueous solution (0 ppm). The ^{11}B MAS NMR spectra of the glasses were acquired at 192.6 MHz with 15 kHz spinning rate. For each sample, 256 acquisitions were obtained with a pulse delay of 3 s and a pulse width of 0.3 µs with a tip angle of 15°. The ^{11}B MAS spectra were corrected and referenced against a 1 M H_3BO_3 aqueous solution at 19.6 ppm. Spectral deconvolution was performed using the dmfit 2002 program with a "Q-mas 1/2" model that includes the assumption of the three boron species to estimate the population and NMR parameters of the boron species. The chemical shift

of ^{11}B is influenced by its first coordination numbers, BO_3 and BO_4. It is necessary to introduce two three-coordinated boron species for ring (B_3O_3 two three-coordinated boron species for ring and non-ring structures) and non-ring structures and four-coordinated boron (BO_4).

A high-energy X-ray diffraction experiment was performed at the BL04B2 beamline at the SPring-8 synchrotron radiation facility (Hyogo, Japan) using a two-axis diffractometer dedicated to the study of the disordered materials.[30] The incident X-ray energy was 61.43 keV ($x = 0$, 1, 2.5, and 5) or 112.79 keV ($x = 10$). The raw data were corrected for polarization, absorption, and background, and the contribution of Compton scattering was subtracted using a standard data analysis software.[30]

Small-angle X-ray scattering spectra were measured at the BL19B2 beamline at SPring-8. The incident X-ray energy was 30 keV, and the exposure duration was 90 s. The camera distance was 3045 mm.

The Zn K-edge (9.66 keV) XAFS spectra were measured using the BL01B1 beamline at SPring-8. The measurements were performed using a Si(111) double-crystal monochromator in transmission mode (Quick Scan method) at RT. Pellet samples for the measurements were prepared by mixing a granular sample with boron nitride. The corresponding analyses were performed using the Athena software.[31]

3. Results and discussion

The chemical composition of the glass was 60ZnO–$(40 - x)P_2O_5$–xB_2O_3 (ZPBx). Since the B_2O_3 fraction is used to replace the P_2O_5 fraction, we refer here as B_2O_3-poor ($x = 1$, 2.5, and 5) and B_2O_3-rich ($x = 10$) glasses. Note that the total number of cations is not changed by the B_2O_3 substitution. The values of T_g increased with increasing B_2O_3 fraction, suggesting that a stronger network was formed by the substitution of B_2O_3 units. Recently, we have reported that cation-based composition is suitable for discussion of phosphate-based low-melting glasses.[32] Although the report suggests that T_g can be approximated to some extent by linear regression,[32] the current T_g values are not proportional to the B_2O_3 fraction, especially in compositions with low B_2O_3 fraction. It suggests that T_g of B_2O_3-poor compositions is dominated by phosphate units. Next, we examine several macroscopic properties of ZPBx glasses using inelastic light-scattering approaches. The values of T_g, molar volume, refractive index, and longitudinal sound velocity V_L are summarized in Table 1, in addition to the longitudinal elastic modulus c_{11} values calculated from the density, refractive index, and longitudinal sound velocity of the ZPBx glasses. **Figure 1**(a) shows the Brillouin scattering spectra of the ZPBx glasses. The Brillouin peak shifted to a higher frequency with an increase in the substituent fraction. Figure 1(b) shows the Brillouin shift ν_B and Brillouin linewidth as a function of B_2O_3 fraction. The molar volumes calculated from the densities of these glasses decreased monotonically with increasing x (Table 1). The decrease in molar volume indicates an increase in the packing density inside the glass.

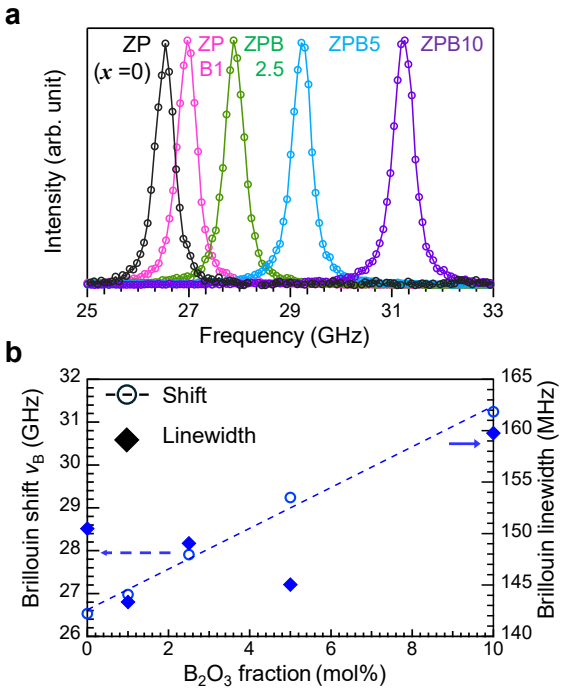

Fig. 1. **Inelastic light scattering spectroscopy of B_2O_3 substituted-ZP glasses I. a** Brillouin scattering spectra of the ZPBx glasses containing different B_2O_3 substitutions. **b** Brillouin shift ν_B (open circles) and the peak linewidth (closed squares) of ZPBx glasses as functions of the B_2O_3 fraction.

Because the elastic modulus reflects the packing density of the components and average bond strength,[33,34] it is assumed that B_2O_3-substitution induces network connectivity with denser packing. On the other hand, the linewidth of the ZPB10 glass is broader than that of other glasses. Since the linewidth reflects the scattering of ultrasonic wave in a matrix, it is assumed that B_2O_3-rich ZPB10 glass contains wider structural distributions.

As probes for amorphous materials, we used other inelastic light scattering spectroscopy and Raman scattering spectra. The boson peak (BP) frequency, υ_{BPmax}, was obtained by fitting the Raman spectra in the BP with a log-normal function:[35]

$$\frac{\chi''(\nu)}{\nu} = \frac{A}{\sqrt{2\pi}\sigma\nu}\exp\left(-\frac{(\ln\nu - \mu)^2}{2\sigma^2}\right), \qquad (1)$$

where ν, e^{μ}, and σ denote the frequency shift, median of the log-normal distribution, and standard deviation of $\ln \upsilon$, respectively. The region of the Raman shift for fitting is from $0.6I_0$ at the lower frequency and $0.85I_0$ at the higher frequency in the normalized spectra, where I_0 denotes peak height of the BPs. **Figure 2**(a) shows the Raman spectra of the ZPBx glasses (closed circles) and fitting curves (solid lines) obtained using a lognormal function. Figure 2(b) shows the BP energy υ_{BPmax} and peak height calculated in the Stokes region of the Raman scattering of the ZPBx glasses as a function of the B_2O_3 fraction. With increasing B_2O_3 fraction, the υ_{BPmax} of the B_2O_3-substituted glasses linearly increased. Contrarily, the peak height initially

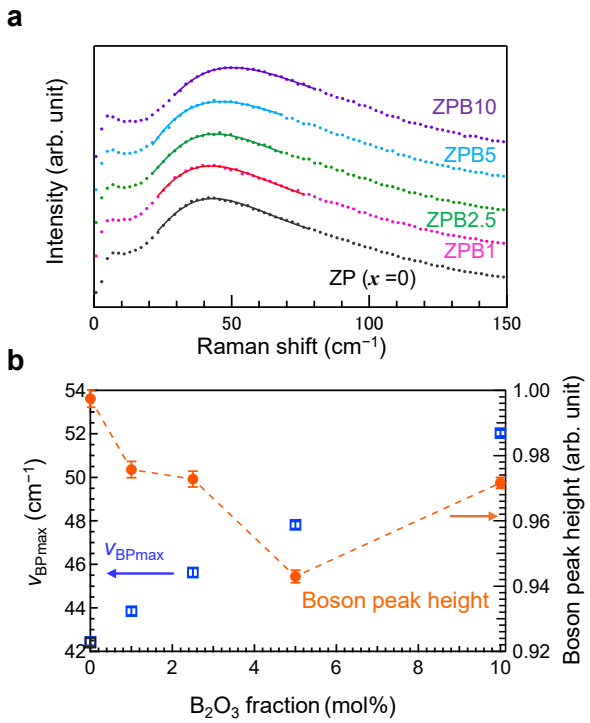

Fig. 2. **Inelastic light scattering spectroscopy of B_2O_3 substituted-ZP glasses II. a** Raman scattering spectra at the boson region of ZPB*x* glasses along with the nonsubstituted ZP glass. **b** Boson peak energy υ_{BPmax} and the peak height of ZPB*x* glasses as a function of the substitution fraction of B_2O_3.

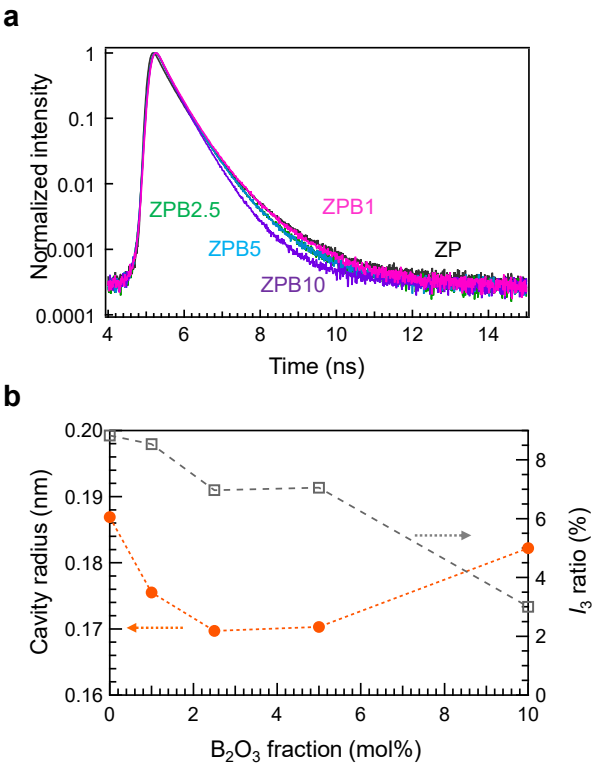

Fig. 3. **Positron annihilation data of ZPB*x* glasses. a** Positron decay curves of ZPB*x* glasses along with ZP glass. **b** Cavity radius and the I_3 fraction of ZPB*x* glass as a function of B_2O_3 fraction.

decreases with increasing B_2O_3 fraction and then increases in the ZPB10 glass. If the origin of the BP does not change, it is expected to observe an inverse relationship over the chemical composition range. This change in BP intensity suggests that the main origin of the BP has changed with more B_2O_3 substitution.

It is expected that the volume ratio and distribution of cavities in glass correlates with the elastic properties.[33] In order to quantify the cavity size, we measure positron annihilation measurement, in which the lifetime of orthopositronium (*o*-Ps) reflects the infomration of cavities in insulators.[36] By fitting, three components can be obtained. The first component I_1 is attributed to the lifetime of parapositronium (*p*-Ps), which has a theoretical value of 125 ps. The second component I_2 is the lifetime of positron annihilated without forming Ps, which also includes the positron decay due to interaction with the Kapton film. The third component I_3 is the reflected lifetime of *o*-Ps. **Figure 3**(a) shows the positron decay curves of the ZP and ZPB*x* glasses. Decay profiles seem to changed depending on the B_2O_3 fraction and the I_3 ratio shown in Fig. 3(b) has a negative correlation with the B_2O_3 fraction. Since I_3 ratios of SiO_2 glass (standard),[37] Li_2O–SiO_2 glass,[37] and SrO–B_2O_3 glass,[38] are approximately 50, 24–31, and 3–15 %, the I_3 ratio is considered to be an indicator for the electron density of materials. However, the calculated cavity radius [Fig. 3(b)] has a complicated change: the radius initially decreases with increasing B_2O_3 fraction and then increases. It indicates that the structures detected by *o*-Ps have been changed.

Considering the effect of B_2O_3 substitution on the structure of ZP glasses, investigation of the coordination state of Zn cations is important because it has been proposed that the subnetwork structures of ZnO_x units in ZnO–P_2O_5 glasses affect their physical properties. In previous reports, the main ZP glass network comprised phosphate chains and small ZnO_x clusters. To examine the average coordination state of Zn, we performed Zn K-edge XAFS measurements on ZP, ZPB5, and ZPB10 glasses. **Figure 4**(a) shows Zn K-edge XANES spectra of ZP, ZPB5, and ZPB10 glasses along with that of ZnO. Although ZP and ZPB5 glasses exhibit similar XANES spectra, the height of white line decreases with increasing B_2O_3 fraction, which correlates with the change of NWF from more ionic glass to more covalent glass. Figure 4(b) shows the $k^3\chi(k)$ of the Zn K-edge EXAFS spectra of these glasses. With an increase in the substitution fraction, the amplitude of the oscillation decreased, indicating that the structural ordering of the ZnO_x units decreased with B_2O_3 substitution. This implies that the ZnO_x units are distorted, or the complicated network structure suppresses the increase in oscillation amplitude. This indicates that the distorted ZnO network was not sensitive to the type of substituted oxide unit. The Fourier transform of the EXAFS spectra of the ZPB*x* glasses is shown in Fig. 4(c), along with that of the reference ZnO. The *k*-region for Fourier transform is from

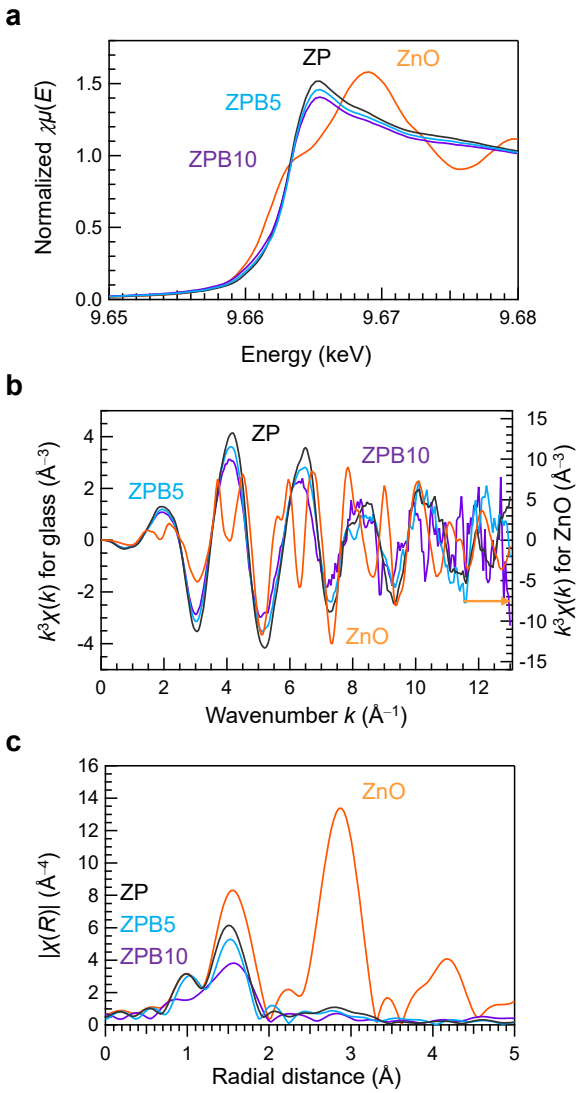

Fig. 4. **Substitution effect of B_2O_3 on the structure of Zn cation. a** Zn K-edge XANES spectra of $60ZnO–40P_2O_5$ (ZP), ZPB5 and ZPB10 glasses along with that of ZnO. **b** Zn K-edge EXAFS spectra of ZP, ZPB5 and ZPB10 glasses along with that of ZnO. **c** Fourier-transform of EXAFS spectra of ZP, ZPB5, and ZPB10 glasses along with that of ZnO.

3.5 to 12 $Å^{-1}$. The disordering caused by the substitution of B_2O_3 causes an apparent decrease in the peak height of the first coordination shell. It is expected that structure of NWF changes depending on the ZnO_x units. To confirm this hypothesis, we measured the local structure of the borate units using MAS NMR spectroscopy.

We then examined the local coordination state of the substituted borate as a counterpart to the change in the phosphate units using MAS NMR spectra. **Figure 5**(a) shows the ^{11}B MAS NMR spectra of ZPBx glasses. The ^{11}B MAS NMR spectra roughly comprise two units: four-coordinated boron $BO_{4/2}$ located around 5 ppm and three-coordinated boron $BO_{3/2}$ observed around 10 ppm.[39–42] Although three-coordinated boron is further classified as ring-structured three-coordinated boron $BO_{3/2\text{-ring}}$ and three-coordinated non-ring boron $BO_{3/2\text{-non-ring}}$, we treat

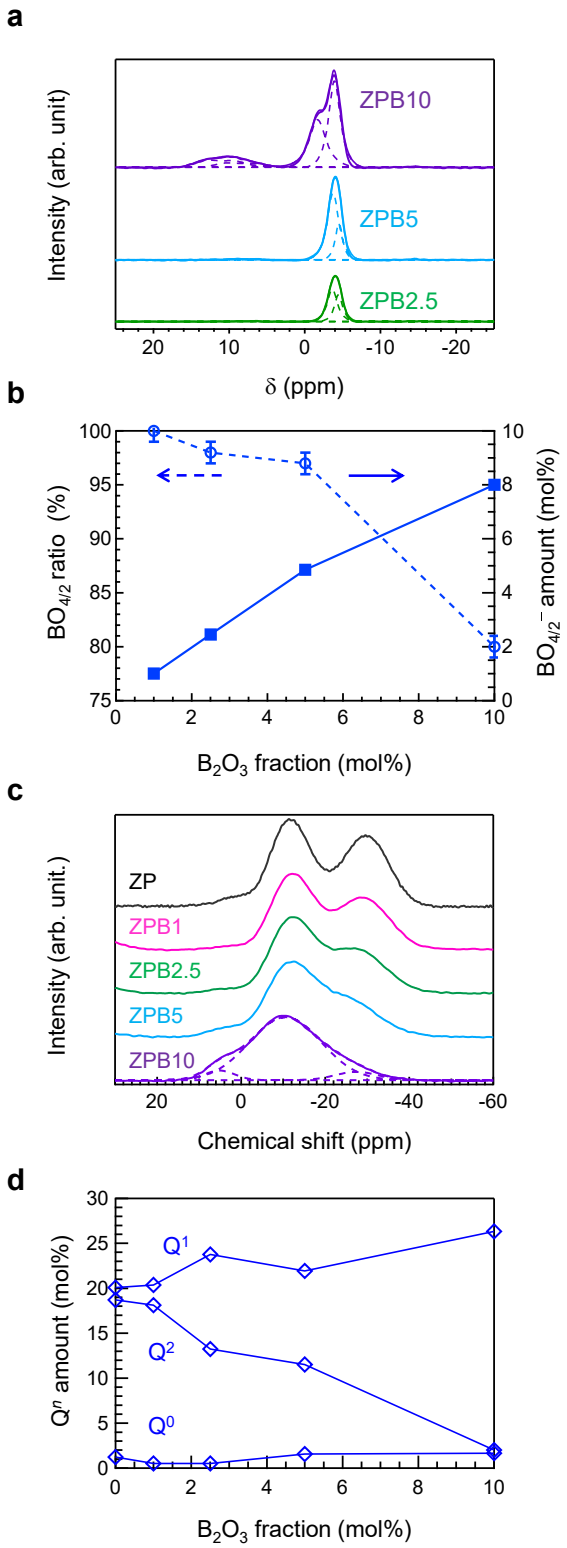

Fig. 5. **B_2O_3-substitution effect of glass structure in MAS NMR measurement. a** ^{11}B MAS NMR spectra of ZPBx containing different B_2O_3 fractions. **b** Change in the $BO_{4/2}$ ratio (left) and $BO_{4/2}$ amount (right) as a function of the B_2O_3 fraction. **c** ^{31}P MAS NMR spectra of ZPBx glasses containing different B_2O_3 fractions. The dashed lines indicate Q^0, Q^1, and Q^2 units of ZPB10 glass after peak deconvolution. **d** Change in the Q^n amount as a function of the B_2O_3 fraction.

$BO_{3/2}$ without further classification. If nearly all boron cations adopt the $BO_{4/2}$ structure, it is expected that the negative charge will be compensated for by the Zn cation near the $BO_{4/2}$ unit, as in ZPB2.5 glass. The presence of $BO_{3/2}$ is observed in the B_2O_3-rich ZPB10 glass. These spectra were deconvoluted using the dmfit 2002 program (dashed lines) to quantitatively discuss the structural changes in borate and to calculate each unit ratio. Figure 5(b) shows the $BO_{4/2}$ ratio (left axis) and $BO_{4/2}$ amount (right axis) as functions of the B_2O_3 fraction. The $BO_{4/2}$ amount is obtained from the product of the $BO_{4/2}$ ratio and the B_2O_3 fraction. Although the $BO_{4/2}$ amount increases with increasing B_2O_3 fraction, the ratio of $BO_{3/2}$ units, which are loosely packed units compared with $BO_{4/2}$, increases. Both the $BO_{3/2}$ and $BO_{4/2}$ units affect the glass network to improve the thermal stability, as shown in Table 1. From ^{11}B MAS NMR, we conclude that the B_2O_3 species work in collaboration with the surrounding matrix, i.e. structural and electronic interactions with phosphate chains and ZnO_x species.

As previously reported, the main network structure of ZP glass consists of phosphate chains. Therefore, we examined the structural changes in the phosphate units using ^{31}P MAS NMR spectroscopy. Figure 5(c) presents the ^{31}P MAS NMR spectra of the ZPBx glasses. The ^{31}P MAS NMR spectra can be decomposed into three units: PO_4^{3-} (Q^0), $PO_{3.5}^{2-}$ (Q^1), and PO_3^- (Q^2).[43] The superscript n indicates the number of bridging oxygen atoms at a phosphorus cation. The dashed lines indicate the units after peak deconvolution. The Q^0 and Q^1 units exhibited delocalized electrons caused by the conjugated P–O$^-$ bonds. Unlike the Q^2 chain, which forms the main glass network, the Q^0 and Q^1 units cannot form a covalent metal–oxygen chain structure.[3–5] From the deconvolution, we can discuss the structural change in the phosphate unit as a function of substitution. Figure 5(d) shows the number of Q^n units, which are obtained by multiplying the ratio of each Q^n unit in each B_2O_3 fraction, as a function of the B_2O_3 fraction. The Q^2 ratio decreases with increasing B_2O_3 fraction, whereas the Q^0 and Q^1 ratios increase. This indicates that the NWF borate units partially substituted the Q^2 phosphate chain network. The Q^2 amounts in both the glasses also decreased.

Here, we discuss the substitutional effect from the viewpoint of the number of bridging oxygen (BO) in the NWF species. Several units belong to the NWF groups: $BO_{4/2}^-$, $BO_{3/2}$ and PO_3^- (Q^2 chain), and the numbers of BO of each unit are 4, 3, and 2, respectively. Based on the hypothesis that network formation is governed by such NWF units, we calculate the total number of BO (N_{BO}) of each unit, which is obtained by the product of the amount of each unit and the ν_{BO}. Using the values in Figs. 5(b) and 5(d), changes in N_{BO} (ΔN_{BO}) of the B_2O_3-substituted system are plotted in **Fig. 6**. Because the absolute values of the increase ($BO_{3/2} + BO_{4/2}^-$) are comparable to those of the decrease (Q^2 chain) in the glass systems, the network-forming units of B_2O_3 work as a linkage of the network instead of the phosphate Q^2 chains. Clear inverse relationships were observed between the increase in the NWF of B_2O_3, suggesting that the decrease in the Q^2 chain and the increase in the NWF units of the B_2O_3 species are inseparable. Furthermore, the coordination states of the constituent B_2O_3 units change depending on the structure of the phosphate network. The obtained data also indicate that the structure of glass is to be discussed based on the cation-based network, not oxide-based composition.[32]

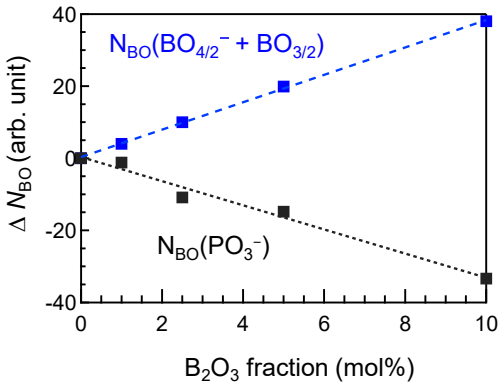

Fig. 6. **Change in the number of borate units and $PO_{4/2}$ (Q^2) unit as a function of the B_2O_3 fraction.** The absolute values of the increase ΔN_{BO} are comparable to those of decrease ΔN_{BO}.

Although monolithic transparent ZPBx glasses were obtained, we assume that a phase separation occurs, especially in the ZPB10 glass. To confirm the tendency, we focused on the X-ray scattering spectra. **Figure 7**(a) shows the X-ray total structure factors $S(Q)$ of the ZP and ZPBx glasses. The peak position of the first sharp diffraction peak (FSDP)[24,25] at $\sim$1.8 Å^{-1} shifts slightly to the higher Q region by B_2O_3 substitution. Our group reported that an increase in the ZnO fraction in ZP glass induces an increase in the packing density due to the formation of ZnO_x polyhedra to form glass network and the cleavage of phosphate chains to be isolated phosphate structures.[22] This shift indicates that the periodicity of the network structure, which is the origin of the FSDP, becomes narrower, that is, a densely packed structure is generated by substitution. It is notable that the $S(Q)$ increases slightly at $<$1 Å^{-1}, especially in ZPB10 glass. Figure 7(b) shows small-angle X-ray scattering spectra of ZPBx glasses along with that of ZP glass. An increase in the intensity in the low-Q region, which is an indicator of phase separation, is clearly observed for the ZPB10 glasses. Similar to the results of X-ray diffraction, the ZPB10 glass exhibits the largest small-angle components, which is consistent with a previous phase separation behavior in Sn^{2+}-doped ZnO–P_2O_5–B_2O_3 glass.[18] It suggests that small-angle scattering measurement is useful for understanding of phase separation of glass,[44] including precipitation of nanocrystallites.

Based on the results, we confirm that atomistic phase separation occurs in ZnO–P_2O_5–B_2O_3 glass with high B_2O_3 substitution. Although apparent macroscopic phase separation was not observed in the B_2O_3-rich glass, atomistic aggregation is detected by several analytical methods. Since atomistic phase separation is thought be an initial

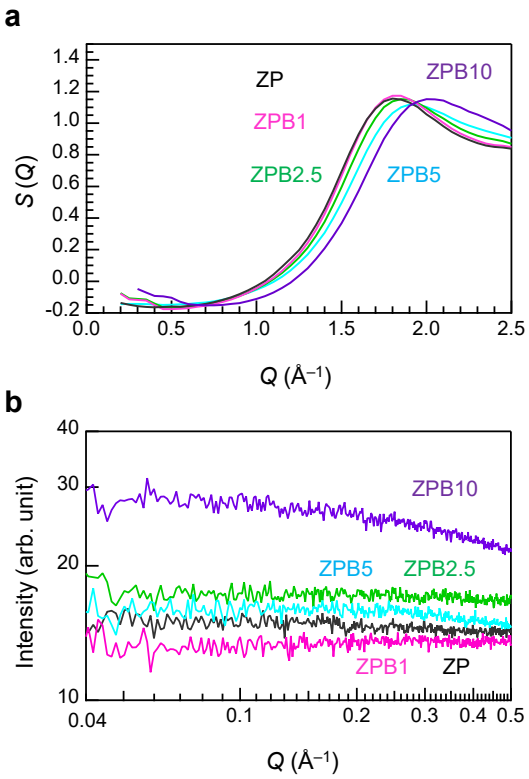

Fig. 7. **Structural analysis using synchrotron X-rays. a** Structure factor $S(Q)$ of ZPBx glasses along with that of ZP glass. **b** Small-angle X-ray scattering spectra of ZPBx glasses along with that of ZP glass.

stage of macroscopic phase separation, the approach will help to understand generation of heterogeneous regions in glass, including precipitation of crystallites.

4. Summary

We examined the structure and physical properties of B_2O_3-substituted $60ZnO–40P_2O_5$ glasses. The substituted B_2O_3 species work as network-forming units that affect closed packing and increase the elastic properties. By comparing the network-forming bridging oxygen, it is suggested that the change in the phosphate chains is a counterpart to the change in the borate unit to maintain the glass-forming network. Although phase separation is not notable at lower B_2O_3-substitution, the formation of clusters is observed in B_2O_3-rich ZP glasses. The formation of cluster observable in small-angle diffraction is consistent with other measurement data in inelastic light scattering and ^{11}B MAS NMR. The formation of heterogeneous region is thought to be atomistic phase separation, which will be a key for understanding of structural change in glass.

Acknowledgements This work was partially supported by the Japan Society for the Promotion of Science Grant-in-Aid for Scientific Research (B) Numbers 18H01714, 22H01785 (H.M.), 21H01018 (Y.F. & A.K.), for Scientific Research (S) Number 19H05618 (A.K.), for Scientific Research (C) Number 24K08045 (Y.F.), and for Transformative Research Areas (A) Numbers 20H05881 (Y.O.), 20H05882 (H.M.), and 23H04096 (T.O.). This work was also supported by the Tokyo Ohka Foundation for The Promotion of Science and Technology. High-energy XRD measurements were performed on the BL04B2 beamline at SPring-8 with the approval of the Japan Synchrotron Radiation Research Institute (JASRI) (Proposal Nos. 2017B0134 and 2024A1023). Zn K-edge XAFS measurements were performed on the BL01B1 beamline at SPring-8 with the approval of the JASRI (Proposal No. 2021A1221). We appreciate the experimental support in XAFS and high-energy XRD measurements by Drs. T. Ina (JASRI) and S. Kohara (NIMS).

Data Availability The authors declare that all relevant data supporting the findings of this study are available from the corresponding author upon request.

References

1) W. H. Zachariasen, *J. Am. Chem. Soc.* 54, 3841 (1932).
2) K. H. Sun, *J. Am. Ceram. Soc.* 30, 277 (1947).
3) J. Brow, *J. Non-Cryst. Solids* 263–264, 1 (2000).
4) U. Hoppe, *J. Non-Cryst. Solids* 195, 138 (1996).
5) R. K. Brow, *J. Non-Cryst. Solids* 194, 267 (1996).
6) R. K. Brow, D. R. Tallant, S. T. Myers and C. C. Phifer, *J. Non-Cryst. Solids* 191, 45 (1995).
7) S. W. Martin, *Eur. J. Sol. State Inor.* 28, 163 (1991).
8) G. Walter, U. Hoppe, J. Vogel, G. Carl and P. Hartmann, *J. Non-Cryst. Solids* 333, 252 (2004).
9) J. W. Wiench, M. Pruski, B. Tischendorf, J. U. Otaigbe and B. C. Sales, *J. Non-Cryst. Solids* 263–264, 101 (2000).
10) U. Hoppe, R. Kranold, A. Barz, D. Stachel, J. Neuefeind and D. A. Keen, *J. Non-Cryst. Solids* 293–295, 158 (2001).
11) G. Walter, U. Hoppe, T. Baade, R. Kranold and D. Stachel, *J. Non-Cryst. Solids* 217, 299 (1997).
12) K. Suzuya, K. Itoh, A. Kajinami and C.-K. Loong, *J. Non-Cryst. Solids* 345–346, 80 (2004).
13) P. Sengupta, *J. Hazard. Mater.* 235–236, 17 (2012).
14) P. I. Paulose, G. Jose, V. Thomas, N. V. Unnikrishnan and M. K. R. Warrier, *J. Phys. Chem. Solids* 64, 841 (2003).
15) J. H. Campbell and T. I. Suratwala, *J. Non-Cryst. Solids* 263–264, 318 (2000).
16) H. Masai, *J. Ceram. Soc. Jpn.* 121, 150 (2013).
17) D. Pugliese, N. G. Boetti, J. Lousteau, E. Ceci-Ginistrelli, E. Bertone, F. Geobaldo and D. Milanese, *J. Alloy. Compd.* 657, 678 (2016).
18) H. Masai, S. Okumura, T. Ohkubo and T. Yanagida, *Opt. Mater. Express* 7, 2993 (2017).
19) M. Shiga, A. Hirata, Y. Onodera and H. Masai, *Commun. Mater.* 4, 91 (2023).
20) S. K. Lee, H. N. Kim, B. H. Lee, H.-I. Kim and E. J. Kim, *J. Phys. Chem. B* 114, 412 (2010).
21) G. Bonny, D. Terentyev, L. Malerba and D. Van Neck, *Phys. Rev. B* 79, 104207 (2009).
22) Y. Onodera, S. Kohara, H. Masai, A. Koreeda, S. Okamura and T. Ohkubo, *Nat. Commun.* 8, 15449 (2017).
23) U. Hoppe, G. Walter, G. Carl, J. Neuefeind and A. C. Hannon, *J. Non-Cryst. Solids* 351, 1020 (2005).

24) Y. Onodera, *J. Ceram. Soc. Jpn.* 130, 627 (2022).
25) S. Kohara, *J. Ceram. Soc. Jpn.* 130, 531 (2022).
26) H. Masai, *J. Non-Cryst. Solids: X* 15, 100105 (2022).
27) H. Masai, T. Tanimoto, T. Fujiwara, S. Matsumoto, Y. Takahashi, Y. Tokuda and T. Yoko, *J. Non-Cryst. Solids* 358, 265 (2012).
28) A. Koreeda and S. Saikan, *Rev. Sci. Instrum.* 82, 126103 (2011).
29) M. Yamawaki, Y. Kobayashi, K. Hattori and Y. Watanabe, *Jpn. J. Appl. Phys.* 50, 086301 (2011).
30) S. Kohara, M. Itou, K. Suzuya, Y. Inamura, Y. Sakurai, Y. Ohishi and M. Takata, *J. Phys.-Condens. Mat.* 19, 506101 (2007).
31) B. Reval and M. Newville, *J. Synchrotron Radiat.* 12, 537 (2005).
32) H. Masai, T. Mihara and K. Kintaka, *J. Ceram. Soc. Jpn.* 131, 466 (2023).
33) T. Rouxel, *J. Ceram. Soc. Jpn.* 130, 519 (2022).
34) A. Masuno, *J. Ceram. Soc. Jpn.* 130, 563 (2022).
35) V. K. Malinovsky, N. Novikov and A. P. Sokolov, *Phys. Lett. A* 153, 63 (1991).
36) R. A. Pethrick, *Prog. Polym. Sci.* 22, 1 (1997).
37) K. Inoue, H. Kataoka, Y. Nagai, M. Hasegawa and Y. Kobayashi, *J. Appl. Phys.* 115, 204903 (2014).
38) H. Masai, T. Ohkubo, Y. Fujii, A. Koreeda, T. Yanagida, T. Ina and K. Kintaka, *Sci. Rep.-UK* 11, 3811 (2021).
39) J. F. Stebbins, P. Zhao and S. Kroeker, *Solid State Nucl. Mag.* 16, 9 (2000).
40) P. Zhao, S. Kroeker and J. F. Stebbins, *J. Non-Cryst. Solids* 276, 122 (2000).
41) M. Vasilescu and S. Simon, *Mod. Phys. Lett. B* 16, 423 (2002).
42) S. Sen, S. Xu and J. F. Stebbins, *J. Non-Cryst. Solids* 226, 29 (1998).
43) R. J. Kirkpatrick and R. K. Brow, *Solid State Nucl. Mag.* 5, 9 (1995).
44) G. N. Greaves, M. C. Wilding, S. Fearn, D. Langstaff, F. Kargl, S. Cox, Q. Vu Van, O. Majérus, C. J. Benmore, R. Weber, C. M. Martin and L. Hennet, *Science* 322, 566 (2008).